

1 **Process contribution to the time-varying residual circulation in tidally**
2 **dominated estuarine environments.**

3

4 *Submission for Estuaries and Coasts*

5

6 **Jennifer M. Brown^{a,*}, Rodolfo Bolaños^b, Alejandro J. Souza^a**

7

8 ^a National Oceanography Centre, Joseph Proudman Building, 6 Brownlow Street, Liverpool, L3
9 5DA, UK.

10 ^b DHI, Agern Allé 5, DK-2970 Hørsholm, Denmark

11 * Corresponding author *Phone:* +44 (0) 151 795 4971, *Fax:* +44 (0) 151 795 4801, *Email:*
12 jebro@noc.ac.uk (J.M. Brown)

13

14 **Abstract**

15 In tide dominated environments residual circulation is the comparatively weak net flow in
16 addition to the oscillatory tidal current. Understanding the 3D structure of this circulation is of
17 importance for coastal management as it impacts the net (longer-term and event-scale) transport of
18 suspended particles and the advection of tracer quantities. The Dee Estuary, northwest Britain, is
19 used to understand which physical processes have an important contribution to the time-varying
20 residual circulation. Model simulations are used to extract the time-varying contributions of tidal,
21 riverine (baroclinicity and discharge), meteorological, external and wave processes, along with

22 their interactions. Under hypertidal conditions strong semi-diurnal interaction within the residual
23 makes it difficult to clearly see the affect of a process without filtering. An approach to separate
24 the residual into the isolated process contribution and the contribution due to interaction is
25 described. Applying this method to two hypertidal estuarine channels, one tide-dominant and one
26 baroclinic-dominant, reveals that process interaction can be as important as the sub-tidal residual
27 process contributions themselves. The time-variation of the residual circulation highlights the
28 impact of different physical process components at the event-scale of tidal conditions (neap and
29 spring cycles) and offshore storms (wind, wave and surge influence). This gives insight into short-
30 term deviation from the typical estuarine residual. Both channels are found to react differently to
31 the same local conditions, with different short-term change in process dominance during events of
32 high and low energy.

33

34 Keywords: Dee Estuary; tide-surge-stratification; POLCOMS-GOTM-WAM; coastal
35 management; residual circulation; hypertidal interaction.

36

37 1. Introduction

38 This research continues from earlier studies of the 3D circulation within the channels of this
39 hypertidal estuary system (Bolaños et al. 2013) and coastal wave impact across Liverpool Bay
40 (Brown et al. 2011). Bolaños et al. (2013) focused on the time-varying stratification and
41 turbulence profiles, in addition to the classification of the different estuarine channels. Here
42 attention is given to the time-varying residual estuarine circulation, which is defined as the
43 instantaneous circulation remaining once the harmonic tide has been removed from the total
44 circulation. The cumulative effect of the event-scale residual circulation within an estuary will

45 influence the net longer-term transport of particles, such as sediment, micro-organisms and
46 biogeochemical particles (nutrients and gasses, e.g. carbon), which are suspended or dissolved in
47 the water column, and the advection of tracer quantities, such as temperature and salinity.
48 Understanding the long-term transport pathways and the event-scale contribution is crucial for
49 sustainable management. Residual circulation is of particular interest as it can determine the
50 sediment pathways controlling long-term morphological evolution of an estuary system (Prandle
51 2004).

52
53 Within coastal areas the tides can interact with variable bathymetry, creating complex residual
54 flow (e.g., Aubrey and Speer 1985; Wang et al. 2009) due to varying depths and bottom friction
55 (e.g., Huthnance 1981; Warner et al. 2004), tidal asymmetries (e.g., Boon and Byrne 1981),
56 intertidal flats (e.g., Bowers and Al-Barakati 1997) and channel constraint (e.g., Brown and
57 Davies 2010). The longitudinal density gradient within an estuary creates a gravitational
58 circulation (Pritchard 1952; Hansen and Rattray 1965), which moves freshwater seaward in the
59 upper water column and salty water landward near the bed; this is particularly important for the
60 net along-channel transport. At times of stratification the strength of this circulation can be
61 increased. Variability in the vertical structure of the residual circulation causes horizontal
62 transport of positively-buoyant particles in the upper flow and negatively-buoyant particles in the
63 bottom flow at different rates (Burchard and Hetland 2010). This residual is further complicated
64 by tidal straining (Simpson et al. 1990) and wind straining (Chen et al. 2009) of the vertical
65 density profile, which can modify the strength of the estuarine circulation. At the coast wave-
66 induced currents can also cause an event-scale residual flow due to mass-transport in the bottom
67 boundary layer (Longuet-Higgins 1958) and radiation stress (Longuet-Higgins and Stewart 1964;

68 Longuet-Higgins 1970). For both tidal and surface waves Stokes' drift can influence the net flow,
69 as well as wind-driven circulation. Depending on the frequency of storm events both wave and
70 wind circulation may contribute to the long-term transport, or create seasonal patterns in the
71 residual.

72
73 Here we investigate the time-varying process contribution to the residual flow within two different
74 channel regimes of the Dee Estuary, situated in Liverpool Bay northwest Britain (Fig. 1). The
75 residuals in these channels represent a tidally-dominant and baroclinically-dominant system
76 (Bolaños et al., 2013). This estuary has contrasting coastlines: one of industrial importance, the
77 other supporting natural habitat. Human intervention within the estuary system, e.g. river
78 canalisation, has led to siltation making the upper estuary un-navigable (Pye 1996). Improved
79 understanding of the sediment pathways within this estuary is therefore of importance for long-
80 term management to sustain the industrial usage and maintain the natural habitat. Here, the 3D
81 circulation influencing sediment transport is made up of the tide and a residual component. A
82 combination of processes and their interactions generate the residual, such as: storm surge,
83 atmospheric forcing, tides, waves, freshwater input and river flow. These processes have been
84 well modelled for the Dee (see Bolaños et al. 2013 and Brown 2010), enabling confident
85 assessment of their influence on the long-term time-mean residual circulation. In the present
86 study a detailed analysis of the time-varying residuals is performed in order to understand the time
87 and depth varying pulses induced for different processes. The modelled time-averaged residual
88 circulation has been validated by Bolaños et al. (2013), while the time-varying residual elevation
89 has been validated by Brown et al. (2012). Here, the modelling system is validated and
90 implemented for selected processes to investigate the event-scale importance of their isolated

91 time-varying contributions to the residual circulation. Using filtering techniques the strength of
92 the sub-tidal and intra-tidal contribution to the residual is assessed.

93
94 In the next section (Section 2) the Dee Estuary is described along with the conditions during the
95 period of study. This is followed in Section 3 by a description of the modelling system and its
96 validation. An approach to separate the residual components of interest is described along with a
97 filtering method to remove tidal interaction. The isolated residual processes and their interactions
98 are presented in Section 4. These time-varying results are used to compare competitive processes
99 to identify how each generates a short-term event-scale contribution to the residual circulation.
100 Following the discussion in Section 5 it is concluded in Section 6 that: in a tidally-dominant
101 channel, under low energy wave and wind conditions, low river flow can generate short-term
102 baroclinic-dominance within the residual circulation. Storm impact is found to have strong
103 influence at the event-scale during extreme conditions. The intra-tidal process residual for this
104 hypertidal estuary is shown to be comparable in magnitude to the sub-tidal process residual. These
105 findings highlight that the short-term (event-scale) residual pathways can differ to the dominant
106 long-term process (Brown et al., submitted). This may be important for net sediment dynamics,
107 since the volume flux can be greatly intensified during certain (storm or river) events.

108

109 2. The study location and conditions

110 2.1 The Dee Estuary

111 The Dee is a hypertidal estuary with semi-diurnal tides reaching a maximum range of ~10 m,
112 creating a vast expanse of intertidal shoals that form a network of tidal channels, within which
113 current speeds can reach 1.2 ms^{-1} (Fig. 2a and b). The estuary experiences low river input (Fig.

114 2e), the mean flow at Manley Hall (a gauging station run by the Environment Agency) between
115 1937 and 2011 was $31 \text{ m}^3\text{s}^{-1}$. Close to the estuary mouth (Fig. 1) two main channels exist, the
116 Welsh Channel to the west and the Hilbre Channel to the east (Bolaños et al. 2011). The waves
117 within the estuary channels are able to reach 2.2 m (Fig. 2c). Typical estuarine stratification close
118 to the mouth occurs in the channels either during (and then persists, Hilbre Channel) or soon after
119 (Welsh Channel) low tide, even though tidal mixing is strong and river discharge is weak. Both
120 channels are strongly influenced by strain induced stratification (Simpson et al. 1990). This is
121 confirmed by calculating the Simpson number ($\sim 1.45 \times 10^{-3}$, Bolaños et al. 2013, equivalent to a
122 Ri_x of ~ 0.6 , Monismith et al. 1996), which is analogous to the horizontal Richardson number, and
123 the Strouhal number ($\sim 5 \times 10^{-4}$, Bolaños et al. 2013, equivalent to a Stokes number of ~ 100 , Souza
124 2013). These values suggest straining of strongly stratified conditions occur when compared with
125 Burchard (2009). As shown by the Ri_x number (> 0.25), even though the river flow is much
126 weaker than the tidal flow the baroclinic influence can be important close to the estuary mouth
127 and tidal straining can be present. Evaluation of this estuary's dynamics (Bolaños et al. 2013) has
128 shown that within this hypertidal system with weak river flow the channels display different
129 dominant behaviours representative of barotropic (Welsh Channel) and baroclinic (Hilbre
130 Channel) dominant environments. The time-mean patterns consist of a vertical 2-layer system in
131 the Hilbre Channel and a horizontal 2-layer system in the Welsh Channel. Even during a period of
132 wind-wave influence the baroclinic 2-layer system still persists in the Hilbre Channel (Brown et
133 al., submitted). The cumulative effect of the time-varying process contribution to the long-term
134 mean spatial pattern in residual circulation is studied further by Brown et al. (submitted). The
135 Kelvin number for the estuary during this study period is 0.97, using the mean density in the
136 channels at the mouth. A value greater than 1 means the Coriolis Effect is important, influencing

137 the baroclinic circulation. This value suggests moderate influence of the Coriolis Effect,
138 explaining why the river influence is dominant in the Hilbre Channel, as the river flow is diverted
139 toward the right of the estuary. This dominance is strengthened by the fact the cross-sectional-
140 average tidal residual is ebb-dominant in Hilbre Channel and flood-dominant in the Welsh
141 Channel (Brown et al., submitted).

142

143 2.2 The study period

144 The time-varying residual circulation is studied at two locations near the mouth of the Dee
145 Estuary. These two points represent the position of instrument deployment for a 25 day period
146 (06:00 14th February – 12:00 9th March 2008) and previous studies (Bolaños et al., 2013) for
147 validation purposes. Details of the instruments deployed are given by Bolaños and Souza (2010).
148 This period includes calm current dominant conditions, prior to the 21st February (< 168 hrs, Fig.
149 2a-c), followed by wave-current conditions, which incorporate an extreme storm event at neap
150 tide creating wave dominant conditions on the 29th February 2008 (359 – 447 hrs, Fig. 2c-e).
151 These changing conditions are therefore appropriate to investigate time-varying residuals using
152 numerical experiments. The use of time-series data at single points enables high frequency time
153 variation (hourly) to be studied, although the spatial variability is not captured. Patterns in the
154 spatial variability of the residual circulation across and along these channels are detailed by
155 Brown et al. (submitted). River discharge reached $52 \text{ m}^3\text{s}^{-1}$ with a mean discharge of $32 \text{ m}^3\text{s}^{-1}$
156 during the study, so is considered as weak (Fig.2e). The Hilbre Channel experienced greater
157 freshwater influence than the Welsh Channel (located in Fig. 1), creating different tidally
158 interactive 2-layer circulation within the channels (Bolaños et al. 2011). Initial studies (Brown et
159 al. 2012) have found residual elevations external to Liverpool Bay and local meteorological

160 forcing are important in influencing the residual water levels within this estuary. Here we
161 investigate the importance of the temporal variability in local and external processes on the 3D
162 residual circulation at the estuary mouth. The findings in the two estuary channels are compared
163 to see how different processes influence a barotropic-dominant and baroclinic-dominant channel.

164

165 3. Model setup and validation

166 3.1 The modelling system

167 The 3D circulation was hindcast by the baroclinic-barotropic Proudman Oceanography
168 Laboratory Coastal Ocean Modelling System (POLCOMS, Holt and James 2001) coupled to the
169 General Ocean Turbulence model (GOTM, Umlauf and Burchard 2005). A further coupling to
170 the WAve Model (WAM, Komen et al. 1994), modified for coastal applications (see Monbaliu et
171 al. 2000) and the generation of radiation stress (using Mellor 2003, 2005), enabled 3D wave-
172 induced currents and enhanced bottom friction and surface roughness to be included. The
173 modelling system was coupled such that a 2-way exchange of information occurred between the
174 component models and was configured to include wetting and drying, making it apt for this
175 estuarine application. The wave coupling was initiated on the 21st February 00:00, when the
176 conditions were no longer considered calm and the waves exceed 0.6 m (> 168 hrs Fig. 2c), to
177 reduce computational cost. No wave induced residual is therefore shown in later figures during the
178 calm period. Prior to this time wave activity is assumed to be minimal within the estuary. Details
179 of the modelling system setup and validation of this period confirming this approach is acceptable
180 are given by Bolaños et al. (2013). Previous studies have also shown it to give good multi-year
181 tide-surge hindcast across the eastern Irish Sea (Brown et al. 2010) and within Liverpool Bay
182 (Brown et al. 2011).

183
184 Operational atmospheric forcing from the UK Met Office was used to drive the local Liverpool
185 Bay model. The full set of ~12 km resolution atmospheric conditions (3 hourly air temperature
186 and specific humidity, with hourly pressure and 10 m wind components) are used to include air-
187 sea heat and momentum fluxes. Freshwater input is considered using daily mean gauged discharge
188 at all available river sources around the Irish Sea. The offshore (Liverpool Bay) model boundary
189 (Fig. 1) was forced by the 1.8 km Irish Sea model (see Brown et al. 2010), so waves and surge
190 generated externally to Liverpool Bay over the continental shelf were able to propagate into the
191 study region. The local wave and surge generation is due to the wind acting over the fetches
192 within the model domain, and atmospheric pressure having an inverse barometer effect. To enable
193 a barotropic-baroclinic Irish Sea simulation, boundary conditions are prescribed by the ~12 km
194 operational European Continental shelf surge model and 3D Atlantic margin model. This then
195 provides the external tide-surge-baroclinic or tide-only current field and elevation boundary
196 conditions every 30 minutes to the Liverpool Bay model, while the wave conditions are updated
197 hourly.

198

199 3.2 Model validation

200 The depth-averaged time-varying residual current components for the default model setup (PG)
201 have been compared with observation (Fig. 3 a and b). Taking the depth-average enables the full
202 water column to be considered at each time instance, and does not incur problems relating to the
203 volume conservation of sigma co-ordinates when time-averaged. The comparison is performed
204 using the ADCP measurements in the Hilbre Channel for the full period of observation at the
205 fixed mooring. Both the model results and observations are filtered (see Section 3.2) to obtain the

206 sub-tidal residual. This technique causes a loss of data at the ends of the time series. It is clear that
207 the model over predicts the depth-mean currents and has less accuracy during the stormier period
208 (around hour 300). Generally the model shows less fluctuation than the observations. The wave
209 conditions are also compared using a wave buoy deployed in the Hilbre Channel close to the
210 ADCP mooring (Fig. 1). The modulation in the wave properties over the tidal cycle in response to
211 depth change is captured (Fig. 3 c and d), while the model tends to slightly under predict the
212 magnitude. Standard error metrics (R^2 coefficient of determination as used by Brown et al. 2013a;
213 *RMS* error and mean Bias as used by Brown et al. 2013b; and the Willmott et al. (1985) index of
214 agreement) are presented in Table 1 for both the residual circulation and waves. Further validation
215 within the bay has been performed on the long-term residual circulation (Polton et al. 2013). The
216 bias in residual circulation near to the Dee Estuary was found to be related to the complex
217 dynamics (miss aligned horizontal density gradient and surface slope) and shallow depths relative
218 to the Ekman layer. The shape of the time-averaged vertical residual circulation profile (validated
219 by Bolaños et al. 2013) is more accurate in the major channel axis component. The profile
220 accuracy is sensitive to both baroclinic and atmospheric forcing, which both have limited
221 accuracy as these forcing conditions are generated from best available large scale model data and
222 limited (daily-averaged) river records. The residual elevation (validated by Brown et al. 2012)
223 does accurately respond to atmospheric forcing, capturing storm events. While the local processes
224 within the estuary contribute little to the residual elevation. The values in Table 1 are therefore
225 considered to be acceptable, since it is difficult to accurately predict residual flow within this
226 complex system with the considered model physics. Since observations in the Welsh Channel are
227 at a single depth below the first model sigma level only the Hilbre Channel has been used for

228 comparison, since this is the more complex channel with baroclinic influence the model is
229 expected to perform as well, if not better, in the tidally-dominant channel.

230

231 3.3 Methods of residual circulation extraction.

232 In hypertidal estuaries the tide has a strong modulating influence on the other non-tidal physical
233 processes, not only due to fast currents ($\sim 1.2 \text{ ms}^{-1}$ during spring tide in the Dee, Fig. 2b), but also
234 due to the wetting and drying of banks, which modifies the bathymetric cross-sectional estuary
235 profile. The model can be used to simulate circulation due to user chosen inputs, for example
236 whether the atmospheric forcing is turned on or not in the model. In this model application the
237 physical processes available for user selection are: meteorological forcing (M), baroclinicity (B),
238 river flow (R), external residual (E), tides (T) and waves (W). Filtering methods are also applied
239 to the model data to remove all energy at tidal frequencies to isolate the tidally-interactive residual
240 component. Here the Chebyshev Type II filter is used as a low-pass filter with a stop-band of 26
241 hours and a pass-band of 30 hours to remove all energy at tidal frequencies. A standard 3 decibels
242 pass-band amplitude was applied with a stop-band attenuation of 30 decibels, which is an
243 attenuation factor of 1000. This leaves only the low frequency (≥ 30 hours, sub-tidal) residual
244 without any tidal energy or tidal interaction, which is removed as it has a similar frequency to the
245 tide. Tidal harmonics with a period ≥ 30 hours will not be removed by this filter design, but within
246 an estuary environment their contribution is expected to be small. A 2-way filtering process was
247 applied so no phase shift occurred in the residual, however the start and end of the residual cannot
248 be accurately obtained, hence a shorter time series is later presented. When applied to the total
249 modelled current velocity more data are lost to filter error, at the ends of the time series, than
250 when applied to the weaker residual current velocities obtained from model simulations. This is

251 because the length of the erroneous period is a percentage of the input signal magnitude. Later
252 figures for the filtered tidal and total current simulations are therefore shorter than those for the
253 filtered (much weaker) residual current. This filter setup has previously been show to successfully
254 remove the tidal energy within surface elevations compared with harmonic tidal analysis methods
255 within this estuary (Brown et al. 2012), so has been used again in this study.

256
257 Here the Liverpool Bay model calculates the current field at 10 vertical levels, represented by
258 sigma coordinates. This has been extracted at the locations of two instrumented fixed moorings
259 deployed in the main tidal channels close to the estuary mouth for this study. Each model
260 simulation within this study has the external boundary conditions prescribed by the Irish Sea
261 model and includes Coriolis. For tide-only no atmospheric or riverine forcing is considered in the
262 modelling systems. For the other reduced physics simulations different component processes are
263 turned off within the Liverpool Bay model, these components included: river flow, baroclinic
264 fields (temperature and salinity gradients), atmospheric forcing and waves. In this model
265 application the classical density-driven flow and straining properties are classified together as the
266 baroclinic processes. The model is therefore coupled as POLCOMS-GOTM-WAM (PGW) or
267 POLCOMS-GOTM (PG) to consider the following processes in the most computationally
268 efficient way: meteorological forcing (M), baroclinicity (B), river flow (R), external residual (E),
269 tides (T), and waves (W) . Metrological forcing (M) represents surface heat and momentum fluxes
270 due to wind, atmospheric pressure and solar heating. Baroclinic processes refer to the temperature
271 and salinity fields setting up density gradients within the model domain. These gradients are
272 generated by river inputs and surface heating. Baroclinicity (B) is included when the time-varying
273 spatial temperature and salinity (density) gradients are enabled within the model. Rivers provide a

274 volume flow rate of freshwater. They can be considered without baroclinicity to provide an
275 additional source of volume flow rate only (R); while baroclinicity is not considered in this case
276 without rivers as a freshwater source. The term ‘external residual’ is used to describe the sub-tidal
277 circulation generated across the Irish Sea that influences the local model domain of Liverpool Bay
278 through boundary forcing. The non-tidal external residual (E) is obtained by removing the tide and
279 the locally generated sub-tidal residuals from the total sub-tidal circulation. In the model, tides
280 (T) are simulated by 15 constituents and shallow water processes are able to influence the
281 propagation of the tidal wave into the estuary. Waves generated over fetches across the Irish Sea
282 enhance both the bottom friction and surface roughness, in addition to generating wave driven
283 currents within the circulation model.

284

285 Prior to any processing, the modelled and observed total velocities (east and north components)
286 were rotated to obtain the major and minor channel axis components (along and across channel
287 components). The rotation was applied separately to the observation and model to prevent
288 discrepancies in bathymetry affecting the rotation. Rotation was applied to each vertical level
289 separately. The largest difference in the rotation angle calculated for each model level and for the
290 depth-averaged velocity was negligible (± 0.7 degrees in the Hilbre Channel). The same angle of
291 rotation, calculated for the reference barotropic-baroclinic simulation (PG_MBRET), was applied
292 to each model simulation for consistency.

293

294 The results presented consider the total residual circulation and its component parts, a sub-tidal
295 (≥ 30 hour period) process driven component and an interactive component due to intra-tidal (< 30
296 hour period) process interaction for all (*i*) processes modelled:

297 $total\ residual = \sum_i (sub\text{-}tidal\ process\ residual + intra\text{-}tidal\ process\ residual).$... (1)

298 From the model simulation the full sub-tidal residual for all processes can be obtained by filtering:

299 $full\ sub\text{-}tidal\ residual = \langle full\ simulation \rangle$... (2)

300 where $\langle \rangle$ denote filtering has been applied. The difference between modelling experiments

301 considering different processes, are used to obtain the time-varying residual circulation due to

302 isolated processes including interactive effects (Table 2). For a single process the process residual

303 obtained from model simulation is:

304 $process\ residual = full\ simulation - reduced\ simulation.$... (3)

305 The sub-tidal residual and intra-tidal residual for that process are then defined as:

306 $sub\text{-}tidal\ process\ residual = \langle full\ simulation - reduced\ simulation \rangle,$... (4)

307 $intra\text{-}tidal\ process\ residual = (full\ simulation - reduced\ simulation) - \langle full\ simulation - reduced\ simulation \rangle,$... (5)

308 For example, the Metrological residual (M in Table 2, row 4) is the difference between a full

309 process model simulation (PGW_MBRET) and a reduced process simulation that does not include

310 Meteorology (PGW_BRET). Filtering this model residual removes any component with a

311 coherent phase, thus removing interaction with intra-tidal frequency between the residual process

312 itself and all other processes considered, mainly the tide. This method extracts the sub-tidal

313 residual induced by the non-tidal process and its nonlinear interactions with other non-tidal

314 forcing. The intra-tidal residual for meteorology is then obtained by subtracting the sub-tidal

315 residual ($\langle PGW_MBRET - PGW_BRET \rangle$) from the process residual ($PGW_MBRET -$

316 PGW_BRET). To obtain the non-tidal sub-tidal residual (Table 1, row 3, Fig. 4 and 5) the

317 difference between a model full physics simulation containing all processes (PGW_MBRETW)

318 and that of the tide only (PG_T) is filtered to remove all intra-tidal iteration.

319

320 In Section 4 the total (sub-tidal and intra-tidal) residual for one or more selected processes is
321 obtained by subtracting a model simulation without the processes in question from one which
322 includes them. The sub-tidal residual is obtained by filtering the total residual and the intra-tidal
323 residual calculated as the difference between the total and sub-tidal residual. By filtering the tide-
324 alone (PG_T, Residual 1) and the fully coupled (PGW_MBRETW, Residual 2) model simulations
325 the sub-tidal (≥ 30 hours) tide-only and full process residual is obtained. This gives an idea of how
326 the tide behaves within the modelled estuary and how it contributes compared with the non-tidal
327 processes to the total residual circulation within the estuary channels.

328

329 4. Results

330 The following figures (4 – 9) show the model data output on sigma levels transformed to depth
331 contours. This transformation creates the semi-diurnal depth oscillation seen in the time-variation
332 of the vertical profile, especially near the surface and less so near the bed. This results from the
333 squeezing and expansion of the vertical profile with tidally induced depth changes and should not
334 be confused as tidal energy remaining in the signal. The transform from Sigma to Cartesian co-
335 ordinates allows the phase of the tide to be seen alongside the time-varying residual.

336

337 4.1 Importance of the tidally generated residual.

338 The modelled tide only (PG_T) and total circulation (PGW_MBRETW) are filtered to remove all
339 semi-diurnal interaction to give the sub-tidal (≥ 30 hrs) residuals. For these two cases, the much
340 larger input signal to the filter causes the data loss at the ends of the time series to be over a longer
341 period than for the weaker residual currents presented later (refer to section 3.2). Comparison of
342 these sub-tidal residuals determines the importance of the tide relative to the non-tidal processes

343 in influencing the total residual circulation. Filtering the tide-alone simulation (PG_T) enables the
344 tidal residual, generated by asymmetries and bathymetric constraint, to be obtained from the
345 model. In both channels the tide causes a long-term (time-averaged) 2-layer horizontal structure
346 (see Bolaños et al. 2013) due to the complexity of the bathymetry and Coriolis (Winant 2008;
347 Zitman and Schuttelaars 2012). At the mooring locations it is shown (Fig. 4 and 5) that the tide is
348 dominant in the Welsh Channel creating a seaward flow, which varies with the spring-neap cycle
349 in the major channel axis component (Fig. 4c); while the major Hilbre Channel axis component
350 (Fig. 4a) shows net landward flow during spring tide and net seaward flow during neaps. In both
351 channels the tidal residual is fastest towards the surface, which is most likely due to less frictional
352 influence from the bed.

353

354 In the Hilbre Channel the tidal time-mean flow is weak with seaward flow on the right and
355 landward flow on the left with flow reversal occurring in the shallow regions towards both banks
356 (Bolaños et al. 2013). The Hilbre mooring is situated to the left of the channel, when facing out to
357 sea, so experiences a landward tidal time-mean flow. The time variation of this flow during
358 different tidal ranges is likely to be in response to the shallow regions of flow reversal changing
359 and also to the weakening of the seaward sub-tidal tidal residual in the Welsh Channel during
360 neap tides. In this channel the tidal residual (Fig. 4a) is about half the magnitude of the sub-tidal
361 residual generated by the combined non-tidal processes (Fig. 6a), considered in the next section.
362 The influence of non-tidal processes on the total (tide plus non-tidal) residual is therefore clearly
363 seen (Fig. 4b).

364

365 In the Welsh Channel a strong seaward flow occurs during spring tide, weakening to zero residual
366 during neap tides (Fig. 4c). The seaward direction of this flow is related to mooring being located
367 on the right side of the channel, when facing out to sea. The time-mean residual within the Welsh
368 Channel has net out flow to the right and net inward flow to the left (Bolaños et al. 2013), with
369 flow speeds more than double that modelled in the Hilbre Channel. At spring tide the magnitude
370 of the Welsh tidal residual is much larger than that due to the non-tidal processes considered, thus,
371 greatly influences the total (tide plus non-tidal) residual at this time (Fig. 4d). However, during
372 neap tide stronger stratification and therefore baroclinicity determines the residual pattern and not
373 the tide, especially during calm atmospheric conditions (> 75 hrs, Fig. 4d). Storm impact,
374 coinciding with neap tide, weakens the stratification modifying the total residual, which becomes
375 storm process driven ($\sim 375 - 450$ hrs, Fig. 4d).

376

377 The same effects as those seen in the major channel axis component occur in the minor channel
378 axis component of both channels (Fig. 5). The Hilbre Channel has a complex sub-tidal residual in
379 the minor channel axis component (Fig. 5b). The surface flow varies in direction from westerly
380 due to baroclinic processes (see Section 4.2) to intense easterly during storm conditions; however
381 the time-mean during calm conditions (< 192 hrs, see Bolaños et al. 2013) of the total sub-tidal
382 residual (Fig. 5b) is weakly toward the east due to wind influence. The balance between baroclinic
383 and meteorological processes is therefore important (as suggested by the large Wedderburn
384 number > 1.6 calculated by Bolaños et al. 2013) when considering how the time-varying residual
385 influences the long-term 3D circulation.

386

387 4.2 The sub-tidal residual contribution

388 The non-tidal sub-tidal residuals (3 – 8 given in Table 2) are analysed to determine the importance
389 of different physical non-tidal process, in contributing to the total residual circulation. In the
390 Hilbre Channel comparison of the non-tidal sub-tidal residual (Figs 6a and 7a) with the total sub-
391 tidal residual (Figs 4b and 5b), shows that non-tidal processes are dominant in both the major and
392 minor channel components, since the subplots are near identical. In the Welsh Channel the major
393 channel axis component of non-tidal sub-tidal residual (Figs 6g) is able to modify the total sub-
394 tidal residual (Figs 4d) during neap tides. While in the minor channel axis the non-tidal sub-tidal
395 residual (Figs 7g) continually influences the total sub-tidal residual (Figs 5d) in the lower water
396 column, in addition to influence over the full depth at neap tide, which is particularly strong
397 during the storm event.

398
399 Figures 6 and 7 show that the non-tidal processes (considered in Table 2, rows 3 – 8) have greater
400 influence in the Hilbre Channel, except for the external surge which has a similar influence in
401 both. Baroclinicity (Figures 6c, and 7c,) is the dominant process at generating sub-tidal residual
402 circulation when all of the considered non-tidal processes are simulated together (Figures 6a and
403 7a). This is seen clearly by the similarity in time-varying pattern. It is important to recall that
404 baroclinicity in this model application represents any process driven by density gradients and their
405 straining. This creates a seaward surface flow and landward bottom flow in the major channel axis
406 component (Fig. 6c). Even at high water, when the water column becomes mixed, straining
407 continues to drive this circulation due to modifications in the flood tide velocity profile and
408 turbulent mixing (Burchard and Baumert 1998), which interacts with the vertical profile of both
409 the river flow and the seaward mass transport in response to Stoke's drift. The tidal straining
410 induced residual therefore has similar characteristics to the classical density-driven flow

411 (Burchard et al. 2011). In the major channel axis the baroclinic residual component (Fig. 6c) is
412 weakened following waves enhancing the seaward flow under windy conditions from the west,
413 both processes reducing stratification (e.g. 300 – 320 hrs), or when the wind is southerly (e.g. 460
414 hrs) and therefore opposing estuarine circulation. The depth of the baroclinic residual surface
415 layer is also found to deepen during the extreme storm once the initially south-westerly winds
416 have veered more westerly (e.g. 380 – 460 hrs).

417
418 In the Welsh Channel the effect of baroclinicity is most noticeable during (neap) current-dominant
419 conditions with southeast winds (the first 100 hours of the study, Fig 6i), even though the river
420 discharge is low and decreasing. Under these conditions stratification is able to form and is
421 strengthened by wind straining. During the extreme storm event the waves (359 – 447 hrs, Figs. 6l
422 and 7l), external surge (captured in the external residual ~400 hrs, Figs. 6k and 7k) and local
423 meteorology (Fig. 6h and 7h) have greatest influence. These processes weaken the stratification in
424 the Welsh Channel and therefore also weaken the persistent density-driven flow pattern (Fig. 6i).

425
426 In both channels the river discharge has the least influence (note the different color scale in Fig.
427 6d, j and 7d, j) creating a weak offshore flow in both channels. The strength of this residual
428 component is related to the river discharge entering the upper estuary from the catchment (Fig. 2e)
429 and not the local storm event itself. Non-regular quasi-period oscillation is seen in the river flow
430 at the mouth (≥ 30 hrs) due to interaction with the atmospheric forcing and possibly the long-
431 period variability in the channel cross-sectional area due to the surge component influencing the
432 total water elevation over the intertidal shoals. The local meteorological (wind) forcing and the
433 external surge seem to have counteractive effects at the event-scale (compare Fig. 6b, h and 7b, h

434 with Fig. 6e, k and 7e, k). The external surge acts to increase water levels causing flow into the
435 estuary during southwest storm events, while the local southwest wind promotes seaward flow for
436 the Hilbre Channel alignment. In the Welsh Channel, these two processes cause opposing
437 bidirectional 2-layer vertical residual flow structures. Finally waves (Fig. 6f, l), when present (>
438 168 hrs, Fig. 2c), typically generate a landward flow in the Hilbre Channel and seaward flow in
439 the Welsh Channel, although this trend reverses with seaward flow near the surface at times of
440 weak southerly winds in the Hilbre Channel and with landward flow near bed in the Welsh
441 Channel at times of storm impact. The wave influence has vertical variability becoming more
442 uniform with depth at times during the extreme storm period (360 – 470 hrs, often related to wind
443 peaks in the Hilbre Channel and the peak wave height in the Welsh Channel). All these processes
444 have clear short-term event-scale influence on the residual circulation.

445

446 The general pattern (Fig. 7a, g) in the minor channel axis residual component is driven by
447 baroclinicity (Fig. 7c, i) and has an easterly bottom flow and westerly surface flow in the Hilbre
448 Channel, and a southerly bottom and northerly surface flow in the Welsh Channel. During storm
449 conditions (e.g. 360 – 470 hrs) the stratification and therefore the minor channel axis baroclinic
450 residual component becomes weaker and other non-tidal process (local wind and less so waves)
451 have greater contribution to total non-tidal residual.

452

453 4.3 The intra-tidal residual contribution

454 The interactions within this hypertidal estuary are predominantly controlled by the tide. The intra-
455 tidal residuals produced by tidal interactions are similar in magnitude to the sub-tidal residuals

456 induced by the non-tidal processes; they are therefore equally as important in contributing to the
457 total (sub-tidal plus intra-tidal) time-varying residual circulation.

458
459 The non-tidal processes (3 – 8 given in Table 2), which have greater influence in the Hilbre
460 Channel also cause a greater intra-tidal (interaction driven) residual within this channel (Fig. 8 and
461 Fig. 9). The interactions generating the intra-tidal residual within Figures 8 and 9 are given in
462 Table 2 (column 4), and are not just due to the tide. Bolaños et al. (2013) shows the importance of
463 tide-stratification interaction within this estuary, which enables periodic stratification to develop at
464 low water followed by its break down creating a well mixed water column at high water.
465 Compared with the non-tidal sub-tidal residuals (Fig. 6 and 7), the intra-tidal residual (Fig. 8 and
466 9), although intermittent, is a significant contribution (at least double at times) to the total residual
467 circulation generated by that process. The intra-tidal residual is of similar magnitude in both the
468 major and minor channel axis components.

469
470 In the Hilbre Channel all of the intra-tidal residuals are generally greater in the upper water
471 column, suggesting tidally dominant interaction with magnitude related to the vertical tidal current
472 profile. In this channel the intra-tidal residual due to all the non-tidal processes (Residual 3, Figs.
473 8a and 9a) is similar to that for baroclinicity in isolation (Residual 5, Figs. 8c and 9c), with
474 additional storm process interaction contributing during the later part of the study period.

475 Apart from the tide and baroclinicity, which have continuous interactive influence, the other
476 processes have more intermittent interactions.

477

478 During the storm event the local meteorology (wind, Residual 4) interacts to create a seaward
479 surface flow at high water elevations and landward surface flow at low water elevation (Fig. 8b
480 and 9b). This interaction is clearly the result of wind straining. At high water slack the estuarine
481 stratification is weakest, but the wind fetches are greatest producing larger wind induced currents.
482 At low water slack stratification is at its strongest, the high wind speeds act to break down the 2-
483 layer system weakening the baroclinic residual circulation enabling the flood tide to have more
484 influence on the surface layers. Strong stratification during low water slack increases the seaward
485 surface flow due to the gravitational circulation. During the flood tide the 2-layer system is broken
486 down, a landward flow occurs at the surface and continues at high water. The river flow (Residual
487 6, Figs. 8d and 9d) interacts with the tide causing a bi-directional flow residual at the mouth. An
488 enhanced seaward flow is caused soon after high water during the ebb current. During low water
489 the river has negligible influence in the Welsh Channel (Figs, 8j and 9j), but can cause a landward
490 flow in the Hilbre Channel as the flood tide starts. At times of high river discharge, a second peak
491 in seaward flow occurs around mid flood tide. In addition to this second seaward river pulse a
492 landward pulse occurs at mid ebb tide. These patterns are more clearly seen in the Hilbre Channel
493 where the river discharge is strongest (e.g. intermittent red and blue stripes in Fig. 8d and 9d,
494 around 300 – 500 hrs).

495
496 In both channels the external residual (Residual 7, Figs. 8e, k and 9e, k) interacts during extreme
497 events, in opposition to the wind. At high water elevations a landward surface flow occurs and at
498 low water elevations a seaward surface flow occurs. The higher water levels at the estuary mouth
499 force more water into the estuary during the periods of weak stratification, which then leaves the
500 estuary during lower water levels by enhancing the seaward surface flow as the 2-layer structure

501 forms. Wave interaction is greatest during wave events (Residual 8, Figs. 8f, l and 9f, l). Wave
502 conditions are greatly controlled by the time-varying depth at the estuary mouth; wave-induced
503 circulation is greatest at high water and is slightly stronger near the surface, causing flow into the
504 estuary. At low water the waves become restricted enabling the typical estuarine surface flow out
505 of the estuary. There is a clear increase in the wave driven current residual during the storm event
506 (at 480 hrs, Figs. 8f, i and 9f, i).

507

508 In the Welsh Channel the interaction for baroclinic processes (Figs. 8i and 9i) and river flow
509 (Figs. 8j and 9j) show the same patterns as those in the Hilbre Channel (Figs. 8c, d and 9c, d, for
510 respective processes) but are weaker. The storm driven processes are also weaker but generate the
511 dominant interactive contribution in this channel. The meteorological intra-tidal residual is the
512 only process which has a reversed influence in Welsh Channel (Fig. 8h) compared with the Hilbre
513 Channel (Fig. 8b). This is due to the channel orientation at the mooring location relative to the
514 southwest wind direction, which drives seaward (northerly) flow in the Hilbre Channel and
515 landward (easterly) flow in the Welsh Channel. Although the Welsh mooring is further towards
516 the open coast, waves have weaker interactive nature with the tide, due to reduced sheltering, by
517 the intertidal banks within the estuary, from the offshore wave activity.

518

519 5. Discussion

520 This paper extends the initial Dee study of Bolaños et al. (2013) to examine the influence of storm
521 impact on the residual circulation, by continuing the study into a period of wave-current
522 conditions. This paper investigates the event-scale time-variation in the vertical residual velocity
523 profile for both a baroclinic and barotropic estuary channel. This gives insight into how the

524 processes interact under different conditions to produce a residual circulation and how the residual
525 changes during different events, such as a wave event or series of neap tides. The 30-day time-
526 mean of the residual is investigated by Brown et al. (submitted) over perpendicular channel cross-
527 sections. They compare equal periods of calm and stormy conditions to identify process
528 dominance over the longer-term, due to the cumulative effect of event-scale process contribution
529 (in magnitude and duration) presented here. The study period (Fig. 2) consists of calm and stormy
530 conditions with a mean river discharge ($32 \text{ m}^3\text{s}^{-1}$), which is equivalent to the long-term mean (31
531 m^3s^{-1}). This period therefore gives good representation of the typical conditions within the Dee
532 Estuary.

533

534 The dynamically evolving bathymetry within the Dee Estuary (Moore et al. 2009) and lack of
535 bathymetric data at the time of observation prevents the time-varying modelled circulation from
536 being perfect at a point observation. In a hypertidal estuary the large tidal prism means inter-tidal
537 shoals in addition to the sub-tidal channels will have an important role influencing the accuracy of
538 the estuarine processes. In Section 3.1 POLCOMS-GOTM is shown to give acceptable
539 simulations of the residual circulation for the given input data (Fig. 3). Previously, the model has
540 been found to be robust at modelling the 3D current patterns within Liverpool Bay (Brown et al.
541 2011; Palmer and Polton 2011) and the Dee (Bolaños et al. 2013). The model is therefore used to
542 understand the contribution of different non-tidal physical process to the time-varying residual
543 current and also the importance of these processes compared with the tide. Although the model
544 results are not a perfect resemblance of the limited observations they do give insight into how
545 estuarine processes interact within this system, demonstrating the important event-scale influence
546 of storms and persistent influence of tidal interaction.

547

548 The presented findings are related to two isolated points, so only give an indication of the residual
549 processes within the studied estuarine channels. These results show the event-scale residual
550 circulation can at times differ from the long-term mean pattern (Brown et al., submitted) and the
551 response to physical events is not constant across the estuary. The time-mean cross-sectional
552 channel profile of these process driven residuals is looked at in more detail by Brown et al.
553 (submitted). Calculation of the exchange flow (see MacCready, 2011) within each channel and the
554 time-mean salt exchange would enable further characterisation of this estuary by determining the
555 residence time and river amplification factor compared with other systems.

556

557 The two studied tidal channels show very different time-varying characteristics. The Welsh
558 Channel is dominated by the tidal residual during spring tide, with baroclinicity having secondary
559 importance, becoming more noticeable during calm neap tide conditions. In this channel extreme
560 southwest storm events occurring at neap tide are able to modify the baroclinically induced residual
561 at this time. However, periods of strong wind and high wave conditions during spring tide have
562 little impact on the dominant tidal residual. Periods of wave activity in the Welsh Channel have
563 large influence on the stratification, greatly reducing the baroclinically induced residual compared
564 with current-dominant periods. This contrasts the Hilbre Channel, in which baroclinicity, through
565 strong straining, is of primary importance, except during extreme southwest storms when local
566 wind has primary importance, and the tide is of a secondary importance. In this channel the non-
567 tidal processes play a much more important role to that of the tide. In the longer-term the total
568 residual has a fairly consistent time-mean pattern for 15-day periods of both calm and stormy
569 conditions (Brown et al., submitted). Events of increased wave activity seems to have less

570 instantaneous influence, possibly due to the more sheltered position of the moored instruments
571 within this channel.

572
573 During storm events the induced process residuals are similar in magnitude to the more typical
574 calm conditions. However, due to their short duration storms are unlikely to have great influence
575 on the long-term residual pattern (Brown et al., submitted). The continuous atmospheric forcing,
576 in particular wind, does influence the vertical (time-averaged, see Bolaños et al. 2013) residual
577 current profile. The influence is greater in the minor channel axis component. For example, the
578 time-varying Hilbre Channel surface residual has a long duration of baroclinic dominance during
579 the study period, driving a weak westerly surface flow (Fig. 5c); while the short period storm
580 event generates an easterly surface flow. However, the long-term (time-average of Fig.9b from 0 –
581 696 hrs, Bolaños et al. 2013) minor channel axis component is towards the east due to the tidal
582 influence on the total residual (Fig. 9b). Future changes in storminess could therefore act to
583 modify the long-term 3D residual current patterns (which are shown by Brown et al., submitted),
584 especially near the surface.

585
586 Strong tidal interaction with the non-tidal processes creates intra-tidal residuals of similar
587 magnitude to the sub-tidal process residuals. This interaction distorts the time-varying residual, so
588 filtering methods are required to clearly identify the sub-tidal process residuals. The difference in
589 dominant processes between the two channels, the strength of the process interactions and spatial
590 variability in the time-mean profile (see Bolaños et al. 2013) demonstrates the complexity of the
591 flow within the estuary and the exchange at the mouth. This implies that the transport of
592 suspended particles is not clear cut within this estuary. The mooring in the Welsh Channel was

593 located towards the right side (when facing offshore), thus experiences one side of the horizontal
594 2-layer structure (Bolaños et al. 2013). It is suggested that within the Welsh Channel the ebb-
595 dominant tidal residual causes a net export of sediment along the right side and is likely (although
596 not studied here) to import sediment along the left side. Within the Hilbre Channel a vertical 2-
597 layer structure (Bolaños et al. 2013), with landward bottom flow is likely to import sediment.
598 Study of the bottom stress across the estuary domain for calm and stormy conditions (Bolaños et
599 al. 2013) demonstrates that although the waves have little influence on the residual circulation
600 they will be an important mechanism for sediment resuspension. In the Welsh Channel where
601 storm impact at neap tide can modify the residual circulation, the direction of wave enhanced
602 sediment transport could influence the net longer-term sediment flux. The interaction of the tidally
603 driven time-variation in wave driven resuspension, controlled by elevation and current direction,
604 will add further complication to the net transport of sediment, which will be the subject of further
605 studies.

606

607 6. Conclusion

608 Modelling enables the time-varying current residual, obtained at all vertical levels at any point
609 within a study region, to be split into process components. Filtering then enables detailed
610 information about the sub-tidal and intra-tidal process contribution to the total current residual to
611 be extracted. This provides useful insight into the non-tidal time-varying process residuals in a
612 hypertidal estuary. Here, the wave-circulation model (POLCOMS-GOTM-WAM) has been
613 applied to the hypertidal Dee Estuary. The model has been validated and used to understand the
614 time-varying current residual for the modelled bathymetry.

615

616 This estuary is known to have a dominant barotropic and baroclinic channel (Bolaños et al. 2013).
617 However, at the event-scale the residual circulation is very variable and each channel is shown to
618 respond differently to short-term forcing conditions. Non-tidal processes dominate the time-
619 varying Hilbre Channel residual under all conditions; with baroclinicity consistently having a high
620 contribution. Within the tidally dominant Welsh Channel the time-varying residual is modified by
621 baroclinicity during low energy conditions (neap tide and calm weather). The tidally-dominant
622 channel at the event-scale (e.g. a period of neap tides) temporarily becoming baroclinically-
623 influenced. Storm driven processes if coincidental with neap tides in this channel also modify the
624 barotropic residual circulation. Storm impact at spring tide has not been captured by this study
625 period. Extreme storms have a strong, but short-term influence during the event. In Liverpool
626 Bay extreme storm surges are often associated with southwest winds, under which conditions the
627 local wind counteracts the influence of the external surge at this estuary mouth. The influence of
628 storm events on the residual circulation is different within the two channels due to their
629 orientation relative to wind direction. This is an example of how the complexity of the channel-
630 bank system within an estuary prevents a consistent pattern in circulation occurring across the
631 estuary. For sediment dynamics the volume flux during such short-term events (e.g. storm events)
632 of atypical circulation may have high impact for the long-term net transport. The short-term
633 deviations in residual circulation demonstrate that time-scales longer than seasonal influence (due
634 to changes in storminess and river discharge) must be considered to truly define the long-term
635 process dominance.

636

637 In addition to the sub-tidal residual the interactions between tide and stratification are found to
638 create a strong intra-tidal residual, influencing the time-variation of the total residual. In

639 hypertidal conditions the interactions must also be included when considering residual circulation
640 as they can be as important as the sub-tidal process contribution itself. The periodic (semi-diurnal
641 for the Hilbre Channel and during calm neap conditions for the Welsh Channel) formation of the
642 vertical 2-layered water column structure can have an important role in longer-term transport
643 pathways. It is therefore suggested that the net transport of suspended and dissolved particles
644 within a hypertidal estuary system can be dependent on the baroclinicity despite low river flow.
645 Management issues related to long-term fluxes and net transport therefore require the careful
646 consideration of the baroclinic influence, even within hypertidal systems. To properly determine
647 residual fluxes at any point within an estuary the full cross-section of the estuary must also be
648 considered. The analysis of MacCready (2011) would be a suitable method to calculate the
649 volume flux through an estuary mouth.

650

651 Acknowledgments

652 The authors would like to thank the reviewers of this manuscript for their very thorough
653 comments helping to focusing the content presented. This research has been carried out as part of
654 Ocean 2025, FORMOST (NERC grant NE/E015026/1), FIELD_AC (EU FP7 program grant
655 242284) and iCOASST (NERC grant NE/J005444/1). The support of the European Commission
656 through FP7, Contract 288710 - MERMAID ("Innovative Multi-purpose offshore platforms: planning,
657 design and operation"), is also acknowledged. John Howarth's help with using low-pass filters was
658 greatly received. Jane Williams (NOC) is thanked for providing the operational surge model
659 output and meteorological (wind and pressure) data, while Clare O'Neill (NOC, COBS) is
660 thanked for providing the offshore temperature and salinity fields to the Irish Sea and
661 supplementing the meteorological forcing with air temperature, humidity, and cloud cover to
662 enable full atmospheric forcing. River data has also been supplied by the Centre for Ecology and

663 Hydrology (CEH) from the UK National River Flow Archive, consisting of the Environment
664 Agency (EA) gauging stations, for the river flow rates around the Irish Sea.

665

666 References:

667 Aubrey, D.G., and P.E. Speer. 1985. A study of non-linear tidal propagation in shallow

668 inlet/estuarine systems, Part 1: observations. *Estuarine Coastal and Shelf Science* 21: 185–205

669 Bolaños, R., and A. Souza. 2010. Measuring hydrodynamics and sediment transport processes in

670 the Dee Estuary. *Earth Systems Science Data* 2: 157–165.

671 Bolaños, R., J.M. Brown, and A. Souza. 2011. Three dimensional circulation modeling in the Dee

672 Estuary. *Journal of Coastal Research* SI (64): 1457-1461.

673 Bolaños, R., J.M. Brown, L.O. Amoudry, and A.J. Souza. 2013. Tidal, riverine and wind

674 influences on the circulation of a macrotidal estuary. *Journal of Physical Oceanography* 43(1),

675 29-50.

676 Boon, J.D., and R.J. Byrne. 1981. On basin hyposmetry and the morphodynamic response of

677 coastal inlet systems. *Marine Geology*, 40(1–2): 27–48.

678 Bowers, D.G., and A. Al-Barakati. 1997. Tidal rectification on drying estuarine sandbanks.

679 *Estuaries* 20(3): 559-568.

680 Brown, J. M., 2010. A case study of combined wave and water levels under storm conditions

681 using WAM and SWAN in a shallow water application. *Ocean Modelling*, 35(3),215-229.

682 Brown, J., R. Bolaños and A. Souza. (submitted) Controls on the medium term estuarine

683 residuals: circulation and elevation. Ocean Dynamics, special issue: PECS 2012: Physics of

684 Estuaries and Coastal Seas, New York, USA, 12-16th August 2012.

685 Brown, J.M., and A.G. Davies. 2010. Flood/ebb tidal asymmetry in a shallow sandy estuary and
686 the impact on net sand transport. *Geomorphology* 114(3): 431–439.

687 Brown, J.M., A.J. Souza, and J. Wolf. 2010. An 11-year validation of wave-surge modelling in the
688 Irish Sea, using a nested POLCOMS-WAM modelling system. *Ocean Modelling* 33(1-2): 118–
689 128.

690 Brown, J.M., R. Bolaños, and J. Wolf. 2011. Impact assessment of advanced coupling features in
691 a tide-surge-wave model, POLCOMS-WAM, in a shallow water application. *Journal of*
692 *Marine Systems* 87(1): 13–24.

693 Brown, J.M., R. Bolaños, M.J. Howarth, and A. Souza. 2012. Extracting sea level residual in
694 tidally dominated estuarine environments. *Ocean Dynamics* 62(7): 969–982.

695 Brown, J.M., L.O. Amoudry, F.M. Mercier, and A.J. Souza, 2013a. Intercomparison of the
696 Charnock and COARE bulk wind stress formulations for coastal ocean modelling, *Ocean*
697 *Science*, 9(4), 721–729.

698 Brown, J.M., R. Bolaños, J. Wolf. 2013b. The depth-varying response of coastal circulation and
699 water levels to 2D radiation stress when applied in a coupled wave–tide–surge modelling
700 system during an extreme storm. *Coastal Engineering*, 82, 102–113.

701 Burchard, H. 2009. Combined effects of wind, tide, and horizontal density gradients on
702 stratification in estuaries and coastal seas. *Journal of Physical Oceanography* 39(9): 2117–
703 2136.

704 Burchard, H., and H. Baumert. 1998. The Formation of Estuarine Turbidity Maxima Due to
705 Density Effects in the Salt Wedge. A Hydrodynamic Process Study. *Journal of Physical*
706 *Oceanography* 28(2): 309–321.

707 Burchard, H., and R.D. Hetland. 2010. Quantifying the contributions of tidal straining and
708 gravitational circulation to the residual circulation in periodically stratified tidal estuaries.
709 *Journal of Physical Oceanography* 40(6): 1243–1262.

710 Burchard, H., R.D. Hetland, E. Schulz, and H.M. Schuttelaars. 2011. Drivers of Residual
711 Estuarine Circulation in Tidally Energetic Estuaries: Straight and Irrotational Channels with
712 Parabolic Cross Section. *Journal of Physical Oceanography* 41(3), 548–570.

713 Chen, S.-N., L.P. Stanford, and D.K. Ralston. 2009. Lateral circulation and sediment transport
714 driven by axial winds in an idealized, partially mixed estuary. *Journal of Geophysical Research*
715 114(C12006): 18pp.

716 Hansen, D. V., and M. Rattray, 1965. Gravitational circulation in straits and estuaries. *Journal of*
717 *Marine Research*, 23, 104–122

718 Holt, J.T., and I.D. James, 2001. An s coordinate density evolving model of the northwest
719 European continental shelf: 1, model description and density structure. *Journal of Geophysical*
720 *Research* 106 (C7):14,015–14,034.

721 Huthnance, J.M. 1981. On mass transports generated by tides and long waves. *Journal of Fluid*
722 *Mechanics*, 102, 367-387

723 Komen, G.J., L. Cavaleri, M. Donelan, K. Hasselmann, S. Hasselmann, and P.A.E.M. Janssen.
724 1994. Dynamics and modelling of ocean waves. Cambridge University Press, Cambridge,
725 532pp.

726 Longuet-Higgins, M.S. 1958. The mechanisms of the boundary layer near the bottom in a
727 progressive wave. Proceedings of the 6th international conference on Coastal Engineering, 184–
728 193.

729 Longuet-Higgins, M.S., and R.W. Stewart. 1964. Radiation stresses in water waves; a physical
730 discussion, with applications. *Deep-sea Research* 11: 529–562.

731 Longuet-Higgins, M.S. 1970. Longshore currents generated by obliquely incident sea waves, 1.
732 *Journal of geophysical research* 75(33): 6778–6789.

733 MacCready, P. 2011. Calculating estuarine exchange flow using isohaline coordinates*. *Journal of*
734 *Physical Oceanography*, 41(6): 1116-1124.

735 Mellor, G. 2003. The three-dimensional current and surface wave equations. *Journal of Physical*
736 *Oceanography* 33(9): 1978–1989.

737 Mellor, G. 2005. Some consequences of the three-dimensional current and surface wave
738 equations. *Journal of Physical Oceanography* 35(11): 2291–2298.

739 Monbaliu, J., R. Padilla-Hernández, J.C. Hargreaves, J.C. Carretero-Albiach, W. Luo, M. Sclavo,
740 and H. Günther. 2000. The spectral wave model WAM adapted for applications with high
741 spatial resolution. *Coastal Engineering* 41(1–3): 41–62.

742 Monismith, S.G., J. Burau, and M. Stacey. 1996. Stratification Dynamics and Gravitational
743 Circulation in Northern San Francisco Bay. In *San Francisco Bay: The Ecosystem*, ed. T.
744 Hollibaugh, American Association for the Advancement of Science, pp. 123–153.

745 Moore, R.D., J. Wolf, A.J. Souza, and S.S. Flint. 2009. Morphological evolution of the Dee
746 Estuary, Eastern Irish Sea, UK: A tidal asymmetry approach. *Geomorphology* 102(4):
747 588–596.

748 Palmer, M.R., and J.A. Polton. 2011. A strain induced freshwater pump in the Liverpool Bay
749 ROFI. *Ocean Dynamics* 61(11): 1905–1915.

750 Polton, J.T., M.R., Palmer, M.J. Howarth. 2013. The vertical structure of time-mean estuarine
751 circulation in a shallow, rotating, semi-enclosed coastal bay: A Liverpool Bay case study
752 with application for monitoring. *Continental Shelf Research* 59:115–126.

753 Prandle, D. 2004. Review: How tides and river flows determine estuarine bathymetries. *Progress*
754 *in Oceanography* 6: 1–26.

755 Pritchard, D. W., 1952. Salinity distribution and circulation in the Chesapeake Bay estuarine
756 system. *Journal of Marine Research*. 15, 33–42.

757 Pye, K. 1996. Evolution of the shoreline of the Dee Estuary, United Kingdom. In: KF Nordstrom,
758 CT Roman (Eds.) *Estuarine Shores: Evolution, Environments and Human Alterations*.
759 John Wiley & Sons Ltd, p14–37.

760 Simpson, J.H., J. Brown, J. Matthews, and G. Allen. 1990. Tidal straining, density currents, and
761 stirring in the control of estuarine stratification. *Estuaries* 13(2):125–132.

762 Souza, A.J. 2013. On the use of the Stokes number to explain frictional tidal dynamics and water
763 column structure in shelf seas. *Ocean Science*, 9:391–398.

764 Wang, B., O.B. Fringer, S.N. Giddings, and D.A. Fong. 2009. High-resolution simulations of a
765 macrotidal estuary using SUNTANS. *Ocean Modelling* 26(1–2): 60–85.

766 Warner, J.C., D.H. Schoellhamer, C.A. Ruhl, and J.R. Burau. 2004. Floodtide pulses after low
767 tides in shallow subembayments adjacent to deep channels. *Estuarine, Coastal and Shelf*
768 *Science* 60(2): 213–228.

769 Willmott, C.J., S.G. Ackleson, R.E. Davis, J.J. Feddema, K.M. Klink, D.R. Legates, J. O’Donnell,
770 and C.M. Rowe. 1985. Statistics for the evaluation and comparison of models. *Journal of*
771 *Geophysical Research* 90(C5): 8995–9005.

772 Winant, C.D. 2008. Three-dimensional residual tidal circulation in an elongated, rotating basin.
773 *Journal of Physical Oceanography* 38(6): 1278–1295.

774 Umlauf, L., and H. Burchard. 2005. Second-order turbulence closure models for geophysical
775 boundary layers. A review of recent work. *Continental Shelf Research* 25(7–8): 795–827.

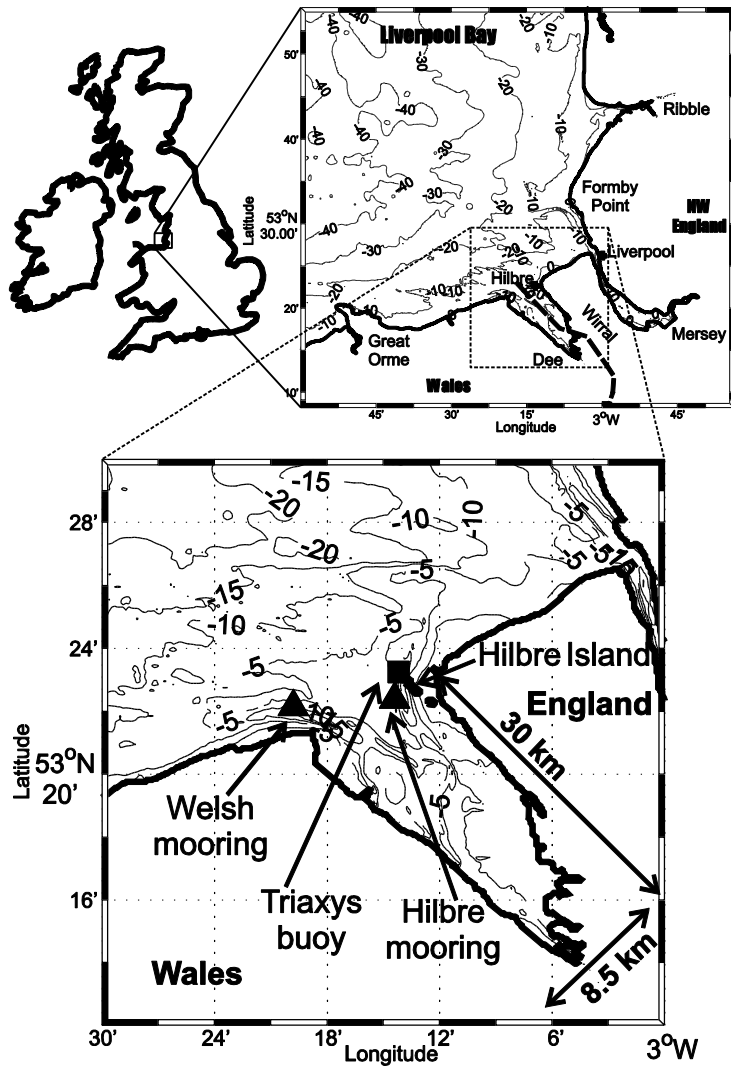
776 Zitman, T.J., and H.M. Schuttelaars 2012. Importance of cross-channel bathymetry and eddy
777 viscosity parameterisation in modeling estuarine flow. *Ocean Dynamics* 62(4): 603–631.

778

779

780

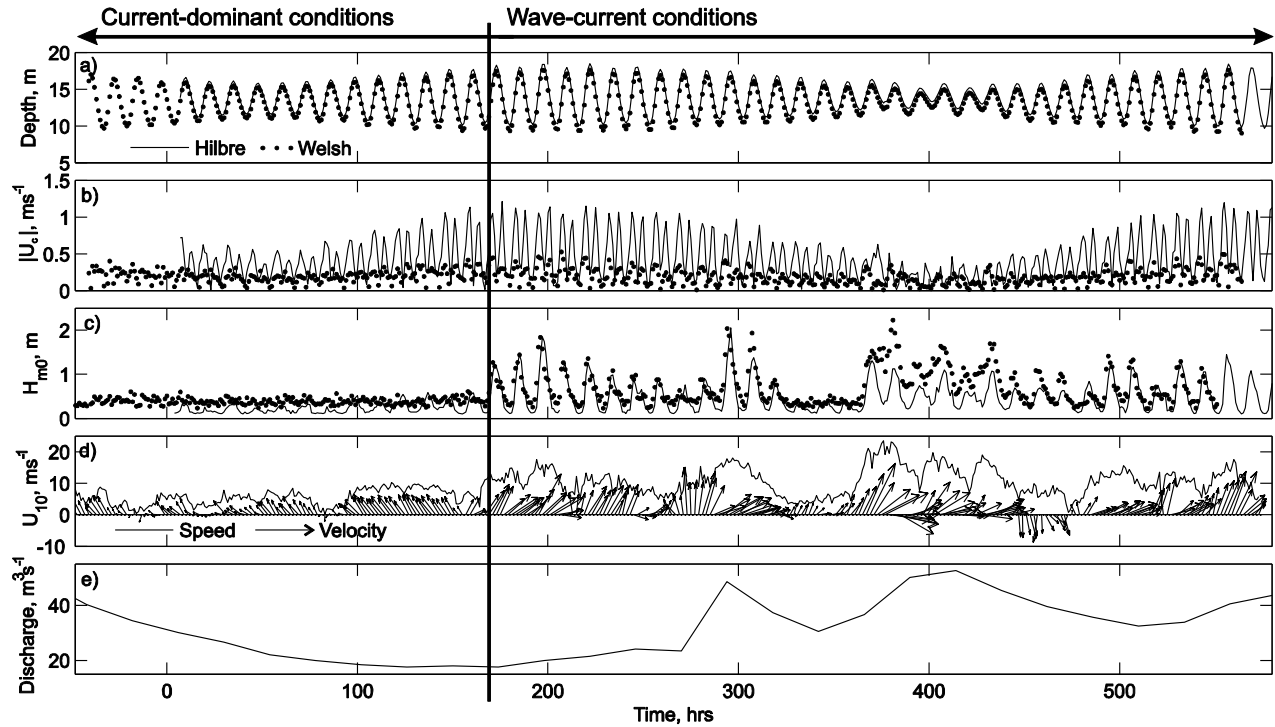
781 **Figure captions:**



782

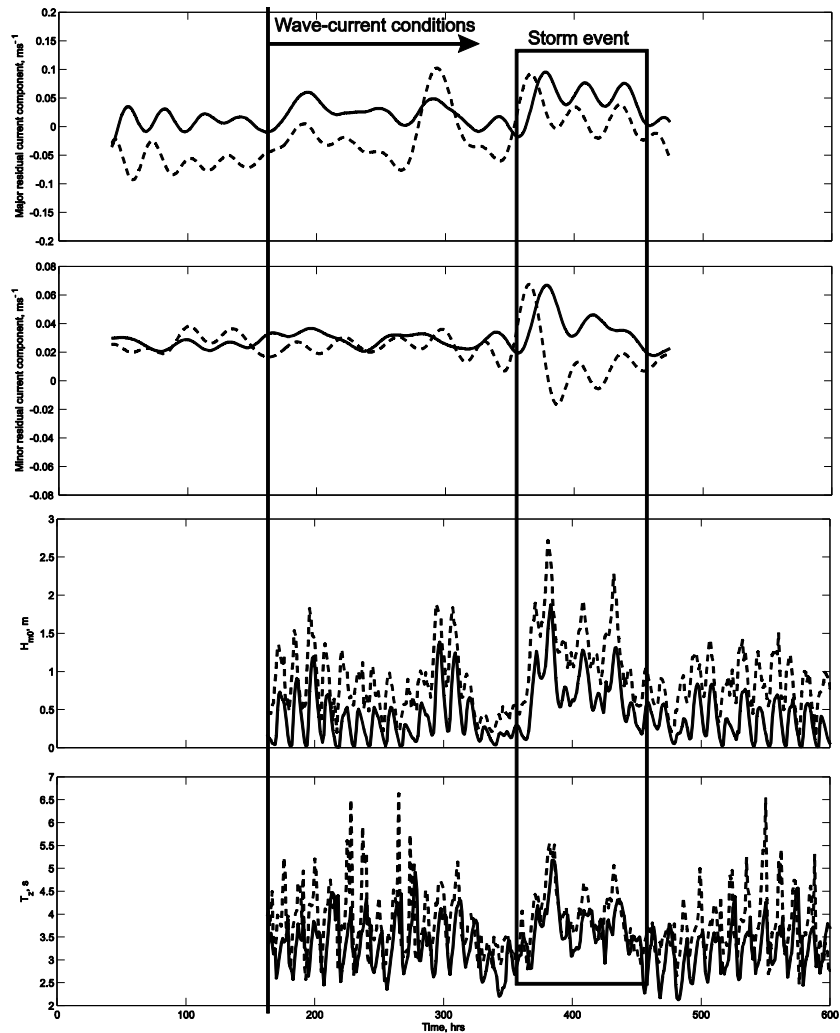
783 Fig. 1 The local Liverpool Bay model domain, northwest Britain. The bottom panel shows the

784 monitoring locations (triangles) and the Triaxys buoy (square) within the Dee Estuary.



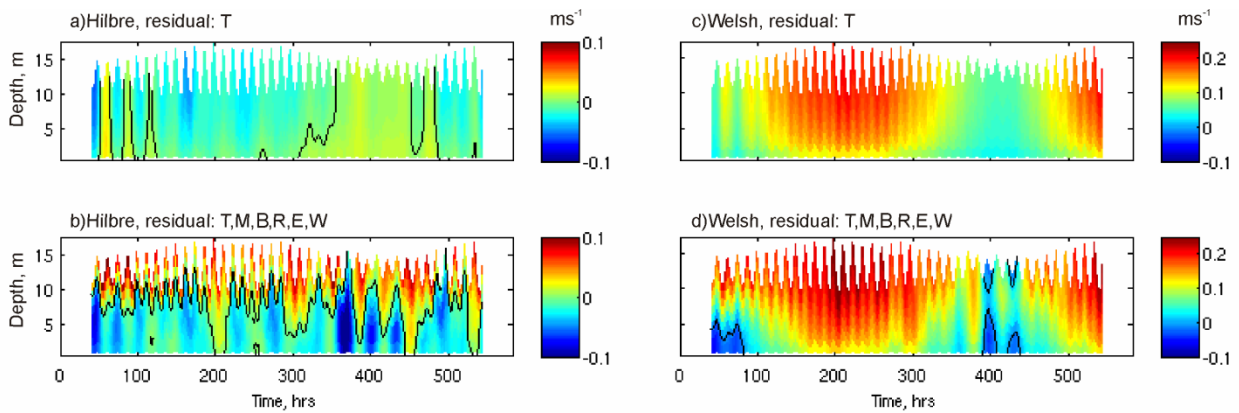
785

786 Fig. 2 The observed conditions during the study period: a) depth measured by the mooring
 787 pressure sensors, b) current speed measured at 0.35 m above the bed in the Welsh Channel
 788 by an ADV (Acoustic Doppler Velocimeter) and at 3.0 m above the bed in the Hilbre
 789 Channel by an ADCP (Acoustic Doppler Current Profiler), c) significant wave height
 790 measured by pressure sensors on the moorings, d) wind conditions at 10 m above the surface
 791 recorded at the Hilbre Island (located in Fig. 1) met station and e) the available daily-
 792 average river discharge for the Dee. The data are shown for both the Hilbre (solid line) and
 793 Welsh (dotted line) Channels. The time axis starts at 06:00 12th February with a 48 hour
 794 delay between the deployment of the Welsh and Hilbre instruments. Time 0 hrs represents
 795 the start of this study when data are available for both channels, 06:00 14th February. Some
 796 data loss for Hilbre occurs during deployment. The vertical line represents when the waves
 797 were initiated within the model.

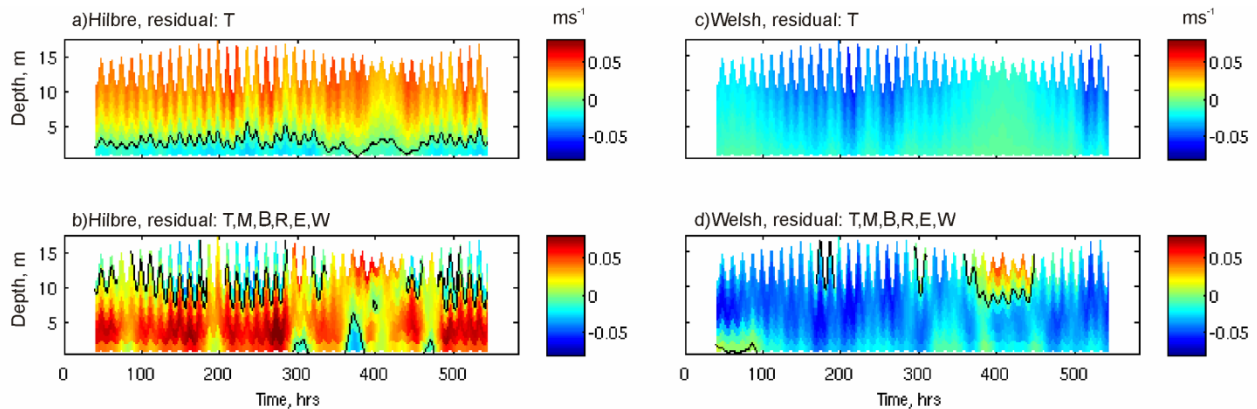


798

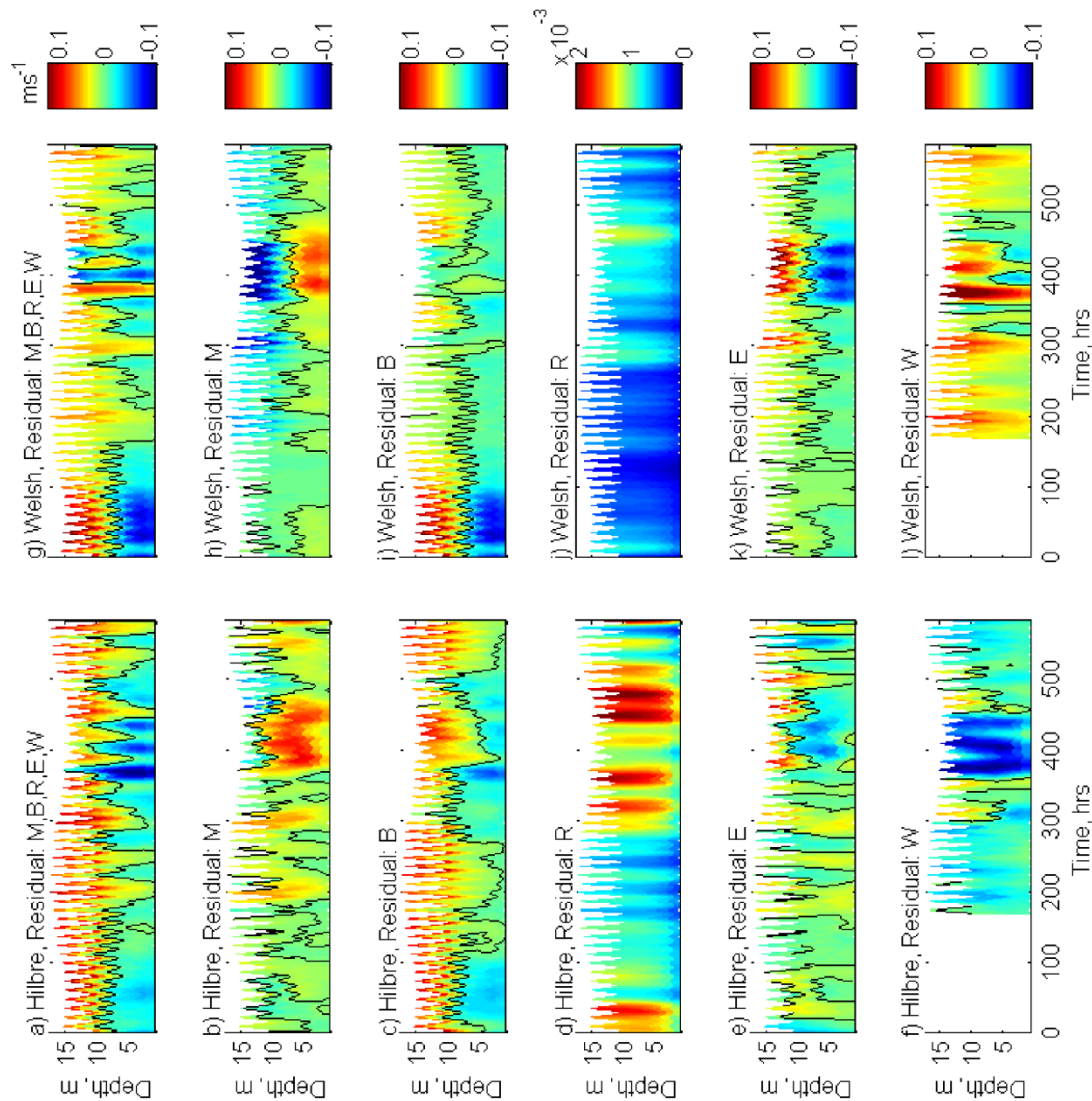
799 Fig. 3 Comparison of the modelled POLCOMS-GOTM and observed ADCP depth-averaged
 800 time-varying filtered residual velocity at the Hilbre mooring for a) the major and b) the
 801 minor channel axis current components. The WAM modelled wave conditions of c) height
 802 and d) period are compared with the Hilbre Triaxys buoy recordings, for the stormy period
 803 (> 21st February). The time axis marks the full study period, 14th February 2008 13:00 – 8th
 804 March 2008 11:00. The solid lines represent model data and the dashed lines observation.
 805 The vertical line represents when the waves were initiated within the model and the box
 806 highlights the extreme storm event.



807
 808 Fig. 4 The major channel axis sub-tidal component of the tidal (top) and total (bottom) residual for
 809 the Hilbre (left) and Welsh (right) Channel mooring locations, Table 2, rows 1 – 2. The data
 810 are obtained at the modelled sigma levels and converted to depth above the bed to show the
 811 tidal variation. The time axis starts at 06:00 14th February 2008. Positive flow is along the
 812 channel out of the estuary. Black line indicates the zero value contours.

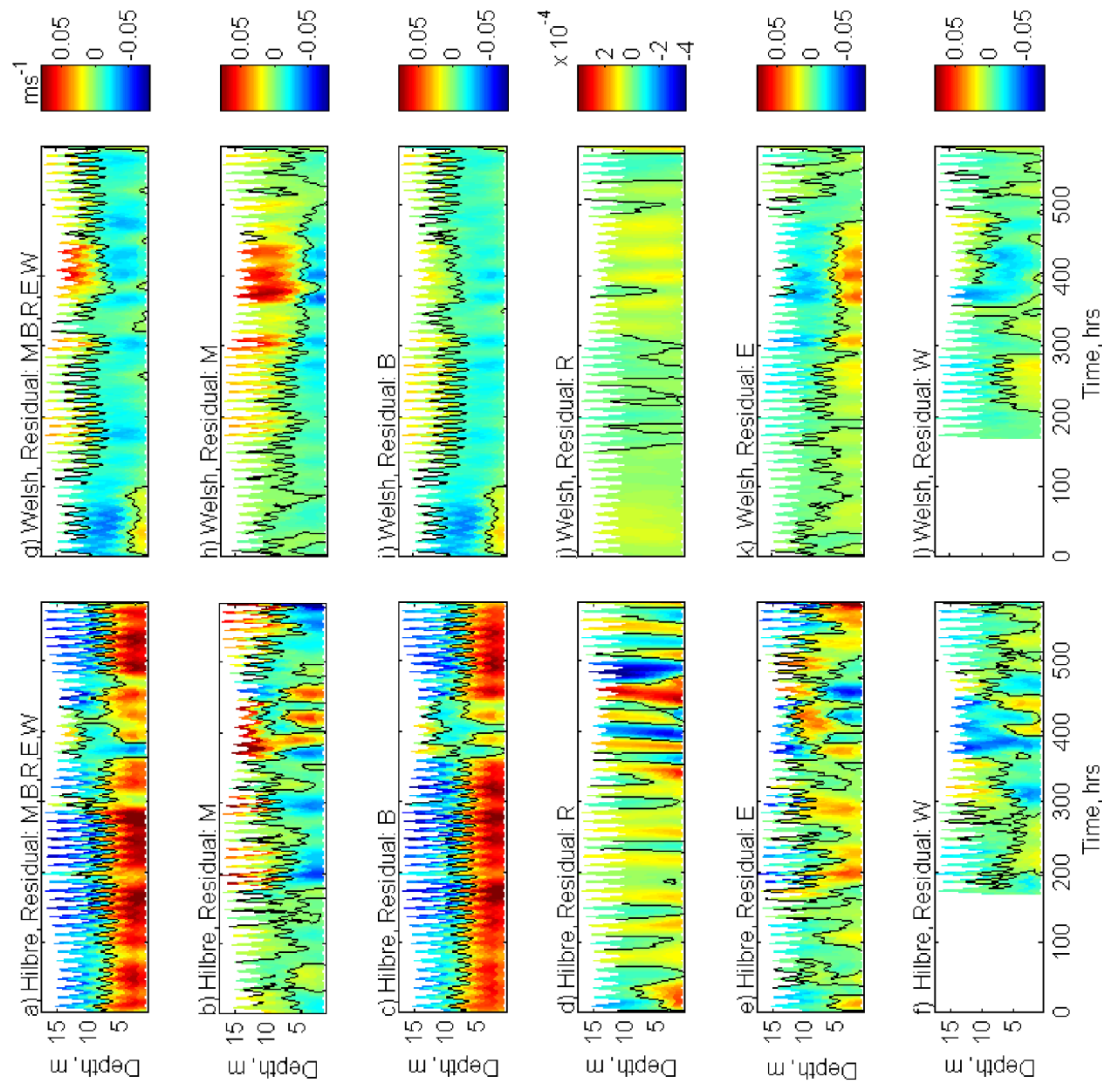


813
 814 Fig. 5 The minor channel axis sub-tidal component of the tidal (top) and total (bottom) residual
 815 for the Hilbre (left) and Welsh (right) Channel mooring locations, Table 2, rows 1 – 2. The
 816 data are obtained at the modelled sigma levels and converted to depth above the bed to show
 817 the tidal variation. The time axis starts at 06:00 14th February 2008. In both channels
 818 positive flow is across the channel from left to right when facing out of the estuary. Black
 819 line indicates the zero value contours.



820

821 Fig. 6 The major channel axis sub-tidal component of the non-tidal model process residuals for
 822 the Hilbre (left) and Welsh (right) Channel mooring locations. The processes considered are
 823 identified in Table 2, row 3 – 8. The data are obtained at the modelled sigma levels and
 824 converted to depth above the bed to show the tidal variation. The time axis starts at 06:00
 825 14th February 2008. Positive flow is along the channel out of the estuary. Note the different
 826 color scale for the residual generated by the river discharge (R, case 6 in Table 2). The black
 827 contour line represents zero velocity.



828

829

Fig. 7 The minor channel axis sub-tidal component of the non-tidal model process residuals for

830

the Hilbre (left) and Welsh (right) Channel mooring locations. The processes considered are

831

identified in Table 2, row 3 – 8. The data are obtained at the modelled sigma levels and

832

converted to depth above the bed to show the tidal variation. The time axis starts at 06:00

833

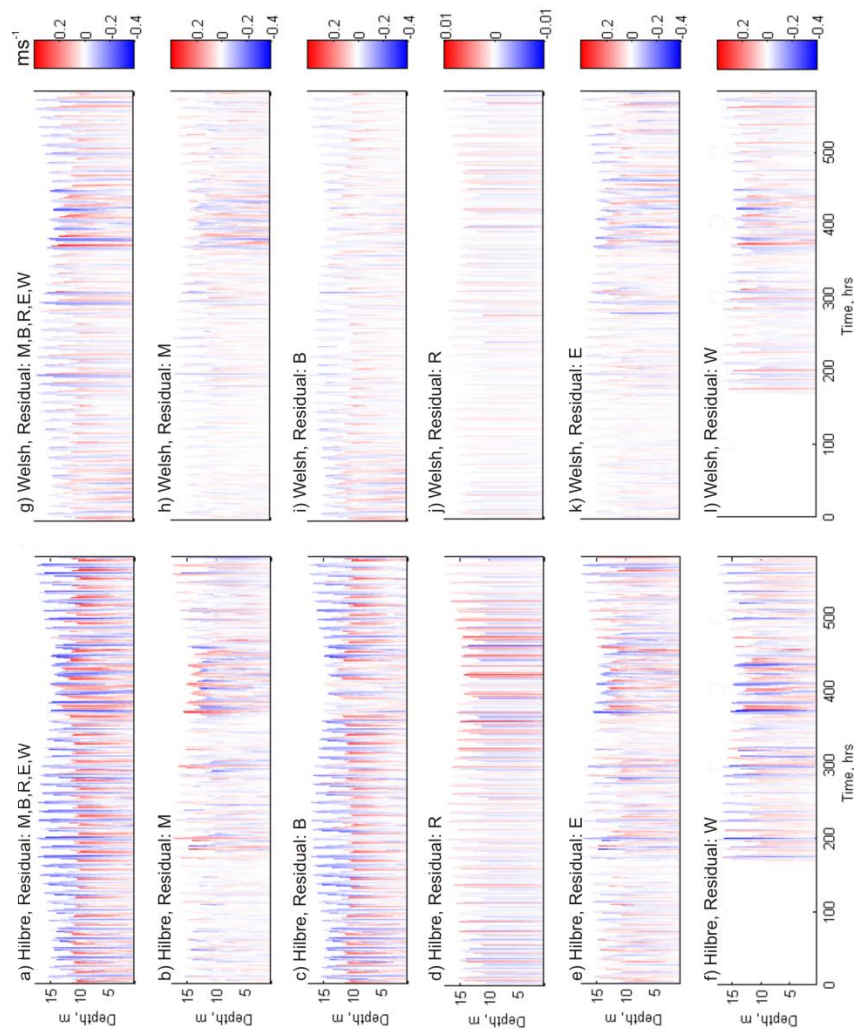
14th February 2008. In both channels positive flow is across the channel from left to right

834

when facing out of the estuary. Note the different colour scale for the residual generated by

835

the river discharge (R, case 6 in Table 2). The black contour line represents zero velocity.



836

837 Fig. 8 The major channel axis component of the modelled intra-tidal residuals for the Hilbre (left)

838 and Welsh (right) Channel mooring locations. The non-tidal processes considered are

839 identified in Table 2, rows 3 – 8. The data are obtained at the modelled sigma levels and

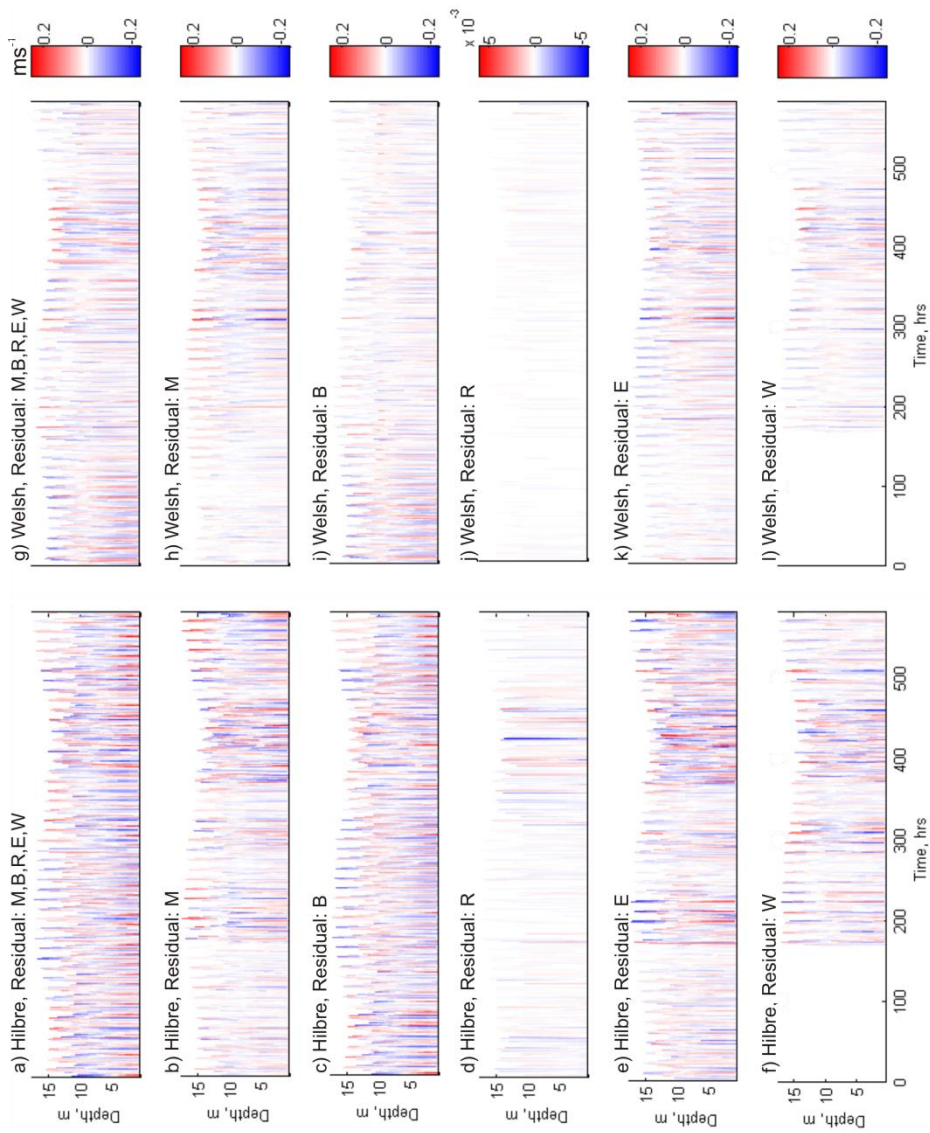
840 converted to depth above the bed to show the tidal variation. The time axis starts at 06:00

841 14th February 2008. Positive flow is an enhancement of the seaward and reduction of

842 landward non-tidal process residual shown in Figure 6 and vice versa for negative flow.

843 Note the different colour scale for the residual generated by the river discharge (R, case 6 in

844 Table 2).



845

846

847

848

849

850

851

852

853

Fig. 9 The minor channel axis component of the modelled intra-tidal residuals for the Hilbre (left) and Welsh (right) Channel mooring locations. The non-tidal processes considered are identified in Table 2, rows 3 – 8. The data are obtained at the modelled sigma levels and converted to depth above the bed to show the tidal variation. The time axis starts at 06:00 14th February 2008. Positive flow is an enhancement of flow towards the right of the channel and reduction of flow towards the left of the channel in the non-tidal process residual shown in Figure 7 and vice versa for negative flow. Note the different colour scale for the residual generated by the river discharge (R, case 6 in Table 2).

854

855 **Table caption:**

856 Table 1 Error metric values of the R^2 , *RMS error*, *mean bias*, and *index of agreement*, for the

857 depth-averaged time-varying residual current components and time-varying wave conditions

858 in the Hilbre channel.

Error metric	Along-channel residual current	Cross-channel residual current	Wave Height	Wave period
R^2	0.26	0.93	0.75	0.34
<i>RMS error</i>	0.06 (m/s)	0.02 (m/s)	0.52 (m)	0.73 (s)
<i>Mean bias</i>	0.05 (m/s)	0.01 (m/s)	-0.47 (m)	-0.45 (s)
<i>Index of agreement</i>	0.56	0.29	0.71	0.67

859

860

861

862

863

864

865

866

867

868

869

870

871

872

873

874 Table 2 The model residuals hindcast by the POLCOMS-GOTM-WAM (PGW) and POLCOMS-
875 GOTM (PG) model, considering the following processes: meteorological forcing (M),
876 baroclinicity (B), river flow (R), external residual (E), tides (T) and waves (W). The
877 processes included in each model residual and the interactions between processes affecting
878 the residual are given.

Residual identity	Model runs subtracted prior to filtering	Processes contribution to the sub-tidal residual	Process and interaction contribution to the intra-tidal residual
1	PG_T – nothing	T	-
2	PGW_MBRETW – nothing	M,B,R,E,W,T	M,B,R,E,W,T
3	PGW_MBRETW – PG_T	M,B,R,E,W	M,B,R,E,W,T
4	PG_MBRET – PG_BRET	M	B,R,E,T,M
5	PG_MBRET – PG_MRET	B	M,R,E,T,B
6	PG_MRET – PG_MET	R	M,T,R,E
7	PG_MBRET – PG_T – Residual 2, 3 & 4	E	B,R,T,E
8	PGW_MBRETW – PG_MBRET	W	M,B,R,E,T,W

879